

Timelike self-similar spherically symmetric perfect-fluid models

Martin Goliath[†], Ulf S Nilsson[†] and Claes Ugglå[‡]

[†] Department of Physics, Stockholm University, Box 6730, S-113 85 Stockholm, Sweden

[‡] Department of Physics, Luleå University of Technology, S-951 87 Luleå, Sweden

Abstract. Einstein's field equations for timelike self-similar spherically symmetric perfect-fluid models are investigated. The field equations are rewritten as a first-order system of autonomous differential equations. Dimensionless variables are chosen in such a way that the number of equations in the coupled system is reduced as far as possible and so that the reduced phase space becomes compact and regular. The system is subsequently analysed qualitatively using the theory of dynamical systems.

Using this approach, we obtain a clear picture of the full phase space and the full space of solutions. Solutions of physical interest, e.g. the solution associated with criticality in black hole formation, are easily singled out. We also discuss the various 'band structures' that are associated with certain one-parameter sets of solutions.

PACS numbers: 0420, 0420J, 0440N, 9530S, 9880H

1. Introduction

Spherically symmetric perfect-fluid models admitting a homothetic Killing vector has attracted considerable attention during the last couple of decades (see, e.g., [1, 2] and references therein). The main reason for this is that the homothetic Killing vector reduces the field equations of spherically symmetric perfect-fluid models from partial to ordinary differential equations. This simplification does not mean that these so-called self-similar models do not contain interesting physical phenomena – quite the contrary. The possibility of violation of the cosmic censorship hypothesis [3] and the existence of sonic surfaces (shock waves) [4, 5] are some examples. The growth of primordial black holes and the evolution of voids can also be studied using self-similar perturbations of the flat Friedmann-Lemaître-Robertson-Walker (FLRW) model [5, 6, 7]. In recent years it has become clear that self-similar models are of crucial importance for the understanding of black hole formation through gravitational collapse. In the full space of spherically symmetric solutions, certain self-similar solutions are separatrices between dispersive solutions and solutions developing black holes [8, 9, 10].

Self-similar spherically symmetric perfect-fluid models exhibit several preferred geometric structures. There are two preferred directions corresponding to the 4-velocity of the fluid and the homothetic Killing vector, respectively. Adapting the coordinates to the 4-velocity of the fluid leads to the ‘comoving fluid approach’ [11, 5, 7, 12, 13]. Adapting the coordinates to the homothetic Killing vector leads to the ‘homothetic approach’ [4, 14]. The spherical symmetry surfaces also constitute a preferred geometric structure. The area of the spherical symmetry surfaces is used as a coordinate in the ‘Schwarzschild approach’ (see, e.g., [3]). There are also some other possibilities, e.g. synchronous coordinate systems and null coordinates, which are useful for discussing singularities [4]. All these approaches are complementary and a full understanding probably relies on a combination of results obtained in the various approaches.

In this paper we will use the diagonal homothetic approach. This has the advantage of yielding equations which are very similar to those of hypersurface homogeneous models. There exists a wealth of literature on how to treat such models. Thus many of the ideas obtained in this area can be carried over into the realm of self-similar spherically symmetric models. However, there are of course disadvantages as well. The symmetry surfaces will in general change causality. Thus, in the diagonal homothetic approach the spacetime has to be covered with two coordinate patches; one for when the homothetic Killing vector is spacelike and one for when it is timelike. Then these two regions must be joined where the homothetic Killing vector is null.

In a previous paper [15] we considered the spatially self-similar (SSS) spherically symmetric models. In the present paper we consider the case of timelike symmetry surfaces, constituting the so-called timelike self-similar (TSS) spherically symmetric models. We obtain a full phase space picture which leads to a more complete understanding of these models than has been previously obtained. Thus the work presented here confirms, corrects and expands the analysis of several authors [3, 4, 7, 9, 10, 12, 13].

The TSS spherically symmetric models are characterized by a four-dimensional homothetic symmetry group H_4 acting multiply transitively on three-dimensional timelike hypersurfaces. The line element, written in diagonal form where one of the coordinates is adapted to the homothetic symmetry, takes the form [4]

$$ds^2 = e^{2t} ds^2 = e^{2t} \left[-D_1^2(x) dt^2 + dx^2 + D_2^2(x) (d\theta^2 + \sin^2 \theta d\varphi^2) \right]. \quad (1)$$

We will consider perfect-fluid models. The energy momentum tensor, \tilde{T}_{ab} , is given by

$$\tilde{T}_{ab} = \tilde{\mu}u_a u_b + \tilde{p}(u_a u_b + g_{ab}), \quad (2)$$

where $\tilde{\mu}$ is the energy density, \tilde{p} is the pressure, and u^a the 4-velocity of the fluid. We will assume

$$\tilde{p} = (\gamma - 1)\tilde{\mu}, \quad (3)$$

as an equation of state where the parameter γ takes values in the interval $1 < \gamma < 2$, which include radiation ($\gamma = \frac{4}{3}$). We have excluded dust ($\gamma = 1$) and stiff fluids ($\gamma = 2$) as they behave quite differently compared to those in the above interval and need special treatment. The dust solutions are explicitly known (these models are just special cases of the general spherically symmetric dust solutions, which are all known explicitly, see, e.g., [16, 1]).

The outline of the paper is the following. In section 2 Einstein's field equations are rewritten in terms of a dimensionless set of variables, in order to obtain a maximal reduction of the coupled system of ordinary differential equations. The variables are chosen so that they take values in a compact phase space. In section 3 the equations are subsequently analysed by using the theory of dynamical systems. In section 4 a numerical investigation is undertaken and global dynamical features are considered. Appendix A describes the properties of the fluid congruence and also the condition for the spacetimes to belong to Petrov type 0. Appendix B gives the relation between various coordinates and the relation between the present variables and other variables used in the literature.

2. The dynamical system

Following [17], we introduce

$$\begin{aligned} D_1 &= B_1^{-1} = e^{\beta^0 - 2\beta^+}, & D_2 &= B_2^{-1} = e^{\beta^0 + \beta^+}, \\ \theta &= 3\dot{\beta}^0, & \sigma_+ &= 3\dot{\beta}^+, \end{aligned} \quad (4)$$

where a dot denotes d/dx . The quantities θ and σ_+ describe the kinematical properties of the normal congruence of the symmetry surfaces in the static (M, ds^2) spacetime that is conformally related to the physical spacetime $(M, d\tilde{s}^2)$ with the homothetic factor e^{2t} (see, e.g., [18]); θ is the expansion while σ_+ describes the shear of the normal congruence of the symmetry surfaces in $(M, d\tilde{s}^2)$. Expressed in an orthonormal frame, the fluid 4-velocity is parametrized by $u^a = (1, u, 0, 0)/\sqrt{1 - u^2}$. Einstein's field equations, $\tilde{G}_{ab} = \tilde{T}_{ab}$, and the equations of motion for the fluid, $\tilde{T}^{ab}_{;b} = 0$, lead to a set of evolution equations for θ , σ_+ , B_1 , B_2 and u . In addition, a constraint equation, and equations for μ_t and $\dot{\mu}_t$ are obtained. The quantity μ_t , related to $\tilde{\mu}$ by

$$\mu_t = \frac{1 + (\gamma - 1)u^2}{1 - u^2} e^{-2t} \tilde{\mu}, \quad (5)$$

is the energy density of the fluid as measured by an observer with a 4-velocity associated with the homothetic symmetry.

As in the SSS case [15], we will now choose to use the $\bar{\theta}, \bar{\sigma}_+$ variables, defined by

$$\begin{aligned} \bar{\theta} &= \frac{1}{\sqrt{3}}(2\theta - \sigma_+), & \bar{\sigma}_+ &= \frac{1}{\sqrt{3}}(-\theta + 2\sigma_+), \\ \theta &= \frac{1}{\sqrt{3}}(2\bar{\theta} + \bar{\sigma}_+), & \sigma_+ &= \frac{1}{\sqrt{3}}(\bar{\theta} + 2\bar{\sigma}_+). \end{aligned} \quad (6)$$

This is done in order to simplify the constraint, while still keeping the quadratic form of the defining equation for μ_t (equation (9) below). This leads to:

Evolution equations

$$\begin{aligned}
\dot{\bar{\theta}} &= -\frac{1}{\sqrt{3}} \left[\bar{\theta}^2 + \bar{\sigma}_+^2 + \bar{\theta}\bar{\sigma}_+ - 3B_1^2 - 3\frac{(\gamma-1)(1-u^2)}{1+(\gamma-1)u^2}\mu_t \right], \\
\dot{\bar{\sigma}}_+ &= -\frac{1}{\sqrt{3}} \left[\bar{\sigma}_+^2 + 2\bar{\theta}\bar{\sigma}_+ + \frac{3}{2}\frac{(3\gamma-2)+(2-\gamma)u^2}{1+(\gamma-1)u^2}\mu_t \right], \\
\dot{B}_1 &= \frac{1}{\sqrt{3}}\bar{\sigma}_+B_1, \\
\dot{B}_2 &= -\frac{1}{\sqrt{3}}(\bar{\theta} + \bar{\sigma}_+)B_2, \\
\dot{u} &= \frac{1-u^2}{\sqrt{3}\gamma[u^2-(\gamma-1)]} \left\{ \gamma[2(\gamma-1)\bar{\theta} + \gamma\bar{\sigma}_+]u \right. \\
&\quad \left. + \sqrt{3}[(\gamma-1)(3\gamma-2) - (2-\gamma)u^2]B_1 \right\}.
\end{aligned} \tag{7}$$

Constraint equation

$$\gamma u \mu_t - \frac{2}{\sqrt{3}}[1 + (\gamma-1)u^2]\bar{\sigma}_+B_1 = 0. \tag{8}$$

Defining equation for μ_t

$$\mu_t = \frac{1}{3} \left[\frac{1 + (\gamma-1)u^2}{u^2 + (\gamma-1)} \right] [\bar{\theta}^2 - \bar{\sigma}_+^2 - 3B_1^2 - 3B_2^2]. \tag{9}$$

Auxiliary equation

$$\begin{aligned}
\dot{\mu}_t &= \frac{\mu_t}{3[1 + (\gamma-1)u^2][u^2 - (\gamma-1)]} \left\{ \sqrt{3}[(4\bar{\theta} + \bar{\sigma}_+)\gamma - 6\bar{\theta}]u^2\gamma \right. \\
&\quad + 6(-7\gamma + 3\gamma^2 + 4)uB_1 - 6(-5\gamma + 2\gamma^2 + 4)u^3B_1 \\
&\quad \left. - \sqrt{3}(\gamma-1)(2\bar{\theta} + \bar{\sigma}_+)u^4\gamma - \sqrt{3}\bar{\sigma}_+\gamma \right\}.
\end{aligned} \tag{10}$$

The defining equation for μ_t shows, assuming non-negative energy density, that $\bar{\theta}$ is a ‘dominant quantity’. Consequently, in order to obtain bounded ‘reduced’ variables, we now introduce $\bar{\theta}$ -normalized dimensionless variables $\bar{\Sigma}_+$, \bar{A} , \bar{K}

$$\bar{\Sigma}_+ = \frac{\bar{\sigma}_+}{\bar{\theta}}, \quad \bar{A} = \frac{\sqrt{3}B_1}{\bar{\theta}}, \quad \bar{K} = 3 \left(\frac{B_2}{\bar{\theta}} \right)^2. \tag{11}$$

The density μ_t is replaced by the density parameter Ω_t , which is defined by

$$\Omega_t = \frac{3\mu_t}{\bar{\theta}^2}. \tag{12}$$

The introduction of a dimensionless independent variable η

$$\frac{dx}{d\eta} = \frac{\sqrt{3}}{\bar{\theta}}, \tag{13}$$

leads to a decoupling of the $\bar{\theta}$ -equation

$$\bar{\theta}' = -(1+q)\bar{\theta}, \quad q = \bar{\Sigma}_+(1 + \bar{\Sigma}_+) - \bar{A}^2 - \frac{(\gamma-1)(1-u^2)}{1+(\gamma-1)u^2}\Omega_t, \tag{14}$$

where a prime denotes $d/d\eta$. The remaining coupled evolution equations can now be written in dimensionless form:

Evolution equations

$$\begin{aligned}
\bar{\Sigma}'_+ &= -\bar{\Sigma}_+ \left[1 - \bar{\Sigma}_+^2 + \bar{A}^2 + \frac{(\gamma-1)(1-u^2)}{1+(\gamma-1)u^2} \Omega_t \right] - \\
&\quad \frac{1}{2} \frac{(3\gamma-2) + (2-\gamma)u^2}{1+(\gamma-1)u^2} \Omega_t, \\
\bar{A}' &= \left[1 + 2\bar{\Sigma}_+ + \bar{\Sigma}_+^2 - \bar{A}^2 - \frac{(\gamma-1)(1-u^2)}{1+(\gamma-1)u^2} \Omega_t \right] \bar{A}, \\
\bar{K}' &= 2 \left[\bar{\Sigma}_+^2 - \bar{A}^2 - \frac{(\gamma-1)(1-u^2)}{1+(\gamma-1)u^2} \Omega_t \right] \bar{K}, \\
u' &= \frac{1-u^2}{\gamma[u^2-(\gamma-1)]} \times \\
&\quad \{ \gamma [2(\gamma-1) + \gamma\bar{\Sigma}_+] u + [(\gamma-1)(3\gamma-2) - (2-\gamma)u^2] \bar{A} \},
\end{aligned} \tag{15}$$

Constraint equation

$$G \equiv \gamma u \Omega_t - 2(1 + (\gamma-1)u^2) \bar{\Sigma}_+ \bar{A} = 0. \tag{16}$$

Defining equation for Ω_t

$$\Omega_t = \frac{1 + (\gamma-1)u^2}{u^2 + (\gamma-1)} (1 - \bar{\Sigma}_+^2 - \bar{A}^2 - \bar{K}). \tag{17}$$

Auxiliary equation

$$\begin{aligned}
\Omega_t' &= \frac{\Omega_t}{[1 + (\gamma-1)u^2][u^2 - (\gamma-1)]} \times \\
&\quad \{ [(4 + \bar{\Sigma}_+)\gamma - 6] u^2 \gamma + 2(-7\gamma + 3\gamma^2 + 4)u\bar{A} \\
&\quad - 2(-5\gamma + 2\gamma^2 + 4)u^3\bar{A} - (\gamma-1)(2 + \bar{\Sigma}_+)u^4\gamma - \bar{\Sigma}_+\gamma \\
&\quad + 2(1+q)[1 + (\gamma-1)u^2][u^2 - (\gamma-1)] \}.
\end{aligned} \tag{18}$$

Equation (9) makes it impossible for $\bar{\theta}$ to change sign when $\mu_t \neq 0$. If $\bar{\theta} > 0$, then $\bar{A} \geq 0$, where we have included the zero boundary value. The field equations are invariant under the transformation

$$(\bar{\Sigma}_+, \bar{A}, \bar{K}, u) \rightarrow (\bar{\Sigma}_+, -\bar{A}, \bar{K}, -u). \tag{19}$$

Thus it is trivial to obtain the case when $\bar{\theta} < 0$ corresponding to $\bar{A} \leq 0$, once the case $\bar{A} \geq 0$ has been analysed. We will therefore assume that $\bar{\theta} > 0$, $\bar{A} \geq 0$. Note that both cases are needed in order to obtain a global picture.

The surfaces defined by $u^2 = \gamma - 1$ are surfaces of non-extendibility of solutions. The only way to cross such a sonic surface analytically is through the line where the numerator of the u' equation of (15) vanishes. This is the *sonic line*. To study the behaviour of trajectories around this line, we make the following non-monotonic change to a new independent variable \aleph ,

$$\frac{d\aleph}{d\eta} = \frac{1}{(\gamma-1) - u^2}. \tag{20}$$

The line element can be obtained when \bar{K} , \bar{A} and $\bar{\theta}$ have been found through the relations

$$D_1 = \sqrt{3}(\bar{\theta}\bar{A})^{-1}, \quad D_2 = \sqrt{3}(\bar{\theta}^2\bar{K})^{-1/2}, \quad x = \sqrt{3} \int \frac{d\eta}{\bar{\theta}}. \tag{21}$$

Table 1. Equilibrium points of the TSS phase space.

Notation	Variables				
	Σ_+	A	K	u	Ω_t
K_+^0	1	0	0	0	0
K_-^0	-1	0	0	0	0
C^0	0	0	1	0	0
T	$-2\frac{\gamma-1}{3\gamma-2}$	0	$\frac{\gamma^2+4(\gamma-1)}{(3\gamma-2)^2}$	0	$\frac{4(\gamma-1)}{(3\gamma-2)^2}$
\tilde{M}^\pm	0	1	0	see text	0
SL		see text		$-\sqrt{\gamma-1}$	
K_+^\pm	1	0	0	± 1	0
K_-^\pm	-1	0	0	± 1	0
M^+	0	1	0	1	0
M^-	0	1	0	-1	0
\mathcal{H}^-		$\bar{\Sigma}_+ + 1$	0	-1	$-2\bar{\Sigma}_+ \bar{A}$
C^\pm	0	0	1	± 1	0

Table 2. Linear analysis of equilibrium points of the TSS phase space.

Notation	Elim.	Eigenvalues			
		λ_1	λ_2	λ_3	λ_4
K_+^0	\bar{A}	$\frac{\gamma-6}{\gamma-1}$	2	$-\frac{3\gamma-2}{\gamma-1}$	
K_-^0	\bar{A}	$-\frac{2-\gamma}{\gamma-1}$	2	$\frac{2-\gamma}{\gamma-1}$	
C^0	-	1	2	-1	-2
T	\bar{A}	$\frac{2-\gamma}{3\gamma-2}$	see text	see text	
\tilde{M}^\pm	\bar{K}	-2	”-	”-	
SL	\bar{K}	0	”-	”-	
K_+^\pm	\bar{A}	4	2	$-\frac{2(3\gamma-2)}{2-\gamma}$	
K_-^\pm	\bar{A}	0	2	2	
M^+	\bar{A}	-4	-2	$-\frac{2(5\gamma-6)}{2-\gamma}$	
M^-	\bar{A}	0	-2	-2	
\mathcal{H}^-	\bar{A}	0	$-2(1+2\bar{\Sigma}_+)$	$-2(1+2\bar{\Sigma}_+)$	
C^\pm	\bar{K}	-1	1	$-\frac{4(\gamma-1)}{2-\gamma}$	

3. Dynamical systems analysis of the reduced phase space

The reduced phase space is determined by $(\bar{\Sigma}_+, \bar{A}, \bar{K}, u)$, related by the constraint $G = 0$, given by equation (16). As in [15], we include the boundary in order to obtain a compact phase space. The boundary is given by a number of invariant submanifolds: $\Omega_t = 0$, $\bar{A} = 0$, $\bar{K} = 0$ and $u = \pm 1$. The constraint cannot be solved globally everywhere. Instead we will follow [17, 19] and solve it locally around the equilibrium points (i.e. we will solve the linearized constraint for different variables at different equilibrium points). This formulation will enable us to achieve a good understanding of the global structure of the dynamics of the reduced phase space. For an introduction to dynamical systems analysis see, e.g., [20], ch 4.

3.1. Equilibrium points and local analysis

There are numerous equilibrium points of the TSS dynamical system. In table 1 the equilibrium points are presented together with Ω_t , which will indicate if a point is on the vacuum boundary $\Omega_t = 0$ or not. Around each equilibrium point we locally eliminate one of the variables by solving the constraint to linear order. In table 2, the variables eliminated in the local analysis are listed together with the eigenvalues

at each point. The equilibrium points are often closely related. Throughout, they are denoted as $\text{Kernel}_{\text{sgn}(\bar{\Sigma}_+)}^{\text{sgn}(u)}$. When there is no risk for confusion we have suppressed $\text{sgn}(\bar{\Sigma}_+)$ or $\text{sgn}(u)$. The kernel indicates the interpretation of the point: M and C refer to Minkowski spacetime; K indicates a Kasner solution; F is the flat FLRW solution and T refers to a static solution discussed below. Note that the self-similar solutions under investigation correspond to orbits in the interior of phase space that asymptotically approach the various equilibrium points. Below, we will comment on some of the equilibrium points.

The equilibrium point C^0 . This point corresponds to the Minkowski spacetime expressed in spherically symmetric coordinates. The constraint surface is degenerate, i.e. $\nabla G = (0, 0, 0, 0)$. Hence we keep all four eigenvalues.

The equilibrium point T . The eigenvalues λ_2 and λ_3 are

$$\lambda_{2,3} = -\frac{1}{2} \pm i \frac{\sqrt{-\gamma^2 + 44\gamma - 36}}{2(3\gamma - 2)}. \quad (22)$$

Note that these eigenvalues are always complex for $1 < \gamma < 2$, and that the real part is always negative. The point T corresponds to a self-similar static solution associated with many names: Tolman [21], Oppenheimer and Volkoff [22], Klein [23] and Misner and Zapsolsky [24]. The same solution also leads to an orbit in the interior phase space, corresponding to a different foliation of the spacetime. This orbit will be referred to as the *static* orbit \ddagger , and will be discussed in section 4.2 below.

The equilibrium points \tilde{M}^\pm . For these points, the variable u takes the values

$$u = \frac{\gamma(\gamma - 1) \pm \sqrt{(\gamma - 1)(\gamma^2(\gamma - 1) + (3\gamma - 2)(2 - \gamma))}}{2 - \gamma}. \quad (23)$$

The expressions for λ_2 and λ_3 will not be given since they are rather complicated. Instead we briefly comment on the stability of the points. At $\gamma = 1$ both points coincide, but as γ increases the points move apart. For $\gamma = \frac{6}{5}$ the point \tilde{M}^+ passes through the point M^+ and leaves the physical part of the TSS phase space. It should be noted that the point \tilde{M}^+ leaves the TSS phase space only to appear in the SSS phase space as one of the points $\pm \tilde{M}$ [15]. The point \tilde{M}^- exists for all values of γ in the interval $1 < \gamma < 2$. It is important to note that \tilde{M}^- always has $-\sqrt{\gamma - 1} < u < 0$, while \tilde{M}^+ always has $u > \sqrt{\gamma - 1}$. This behaviour can be seen in figure 2 (c) - (f). All eigenvalues are negative in the interval $1 < \gamma \leq \frac{6}{5}$ for \tilde{M}^+ . Thus this point is always an attractive node. For \tilde{M}^- two eigenvalues are negative and the third is positive in the interval $1 < \gamma < 2$. Hence this point is a saddle with one outgoing eigendirection.

The equilibrium points SL . The flows are opposite to each other on the different sides of the sonic surfaces at $u^2 = \gamma - 1$. Thus it follows that orbits, in general, cannot pass through these surfaces continuously. It is only possible to cross a sonic surface along the sonic lines SL , where the numerator of the u' equation in (15) vanishes. These lines are defined by

$$\bar{A} = \frac{(-)}{+} \frac{\gamma(2(\gamma - 1) + \gamma\bar{\Sigma}_+)}{4(\gamma - 1)^{3/2}}, \quad u = \frac{(+)}{-} \sqrt{\gamma - 1}, \quad (24)$$

\ddagger In [15], it was called the ‘TOVKMZ’ orbit.

where the lines of equilibrium points are parametrized by $\bar{\Sigma}_+$. The signs within parentheses correspond to the line for which $u = +\sqrt{\gamma-1}$. This line of equilibrium points is located outside the physical phase space for $1 < \gamma < 2$. Consequently the only relevant sonic line is the one at $u = -\sqrt{\gamma-1}$. Using the ‘shock-adapted’ independent variable defined in (20) yields the eigenvalues λ_2 and λ_3 , which are solutions to the equation

$$4(\gamma-1)\lambda^2 + (2-\gamma)(b\lambda + c) = 0, \quad (25)$$

where

$$\begin{aligned} b &= -2\gamma(2(\gamma-1) + \gamma\bar{\Sigma}_+), \quad c = (2-\gamma)[c_1\bar{\Sigma}_+^2 + c_2\bar{\Sigma}_+ + c_3], \\ c_1 &= 7\gamma^3 - 38\gamma^2 + 36\gamma - 8, \quad c_2 = 8(\gamma-1)(2\gamma^2 - 7\gamma + 4), \\ c_3 &= -4(2-\gamma)(\gamma-1)^2. \end{aligned} \quad (26)$$

An analysis of the stability of the line shows that it splits into four parts, see figure 1. The boundaries of the physical interval of the line are determined by $\bar{A} = 0$ and $\bar{K} = 0$. The line is a saddle at $\bar{A} = 0$, then it turns into an attractive node containing the static orbit, discussed in section 4.2. This attractive nodal region is called the S.a.n. region. The eigendirection associated to the eigenvalue with the smaller absolute value dominates the dynamics close to the sonic line [14]. This direction is called the *primary* eigendirection. The other direction is referred to as the *secondary* eigendirection. Subsequently, the eigenvalues become complex and the stability changes to an attractive focus. Orbits approaching the sonic line in this region will spiral and hit the sonic surface infinitely many times, and are thus unphysical [4]. Finally, the stability changes back to an attractive node, now containing the flat FLRW orbit, discussed in section 4.2. This attractive nodal region will be called the F.a.n. region. The behaviour along the sonic line is similar for all values of γ in the interval $1 < \gamma < 2$. Note that the stability is with respect to the new independent variable defined in (20). In the following, if not explicitly pointed out, all figures and discussions of phase space flows are with respect to the original independent variable. Note that there appears to be an error in the stability analysis of Bogoyavlensky, which leads to an erroneous picture of the flow on the phase space boundary [4]. At the boundaries of the focal region, the two non-zero eigenvalues are equal. These *degenerate nodes* will be denoted S.d.n. and F.d.n., respectively. For $\gamma = \frac{4}{3}$, both the static orbit and the flat FLRW orbit coincide with the corresponding degenerate nodes on either side of the focal region.

The equilibrium point M^+ . Note the change in stability of this point at $\gamma = \frac{6}{5}$. This bifurcation corresponds to when the point \tilde{M}^+ passes through M^+ , leaves the TSS phase space and enters the SSS phase space.

The equilibrium points \mathcal{H}^- . This line of equilibrium points is an artifact of the diagonal homothetic approach. It is associated with a causality change of the homothetic vector field. To obtain a global picture, one needs to match the TSS phase space with the SSS phase space. For the choice $\bar{\theta} > 0$ ($\bar{\theta} < 0$), \mathcal{H}^- corresponds to the line of equilibrium points $+\mathcal{H}^-$ ($-\mathcal{H}^+$) in the SSS phase space [15].

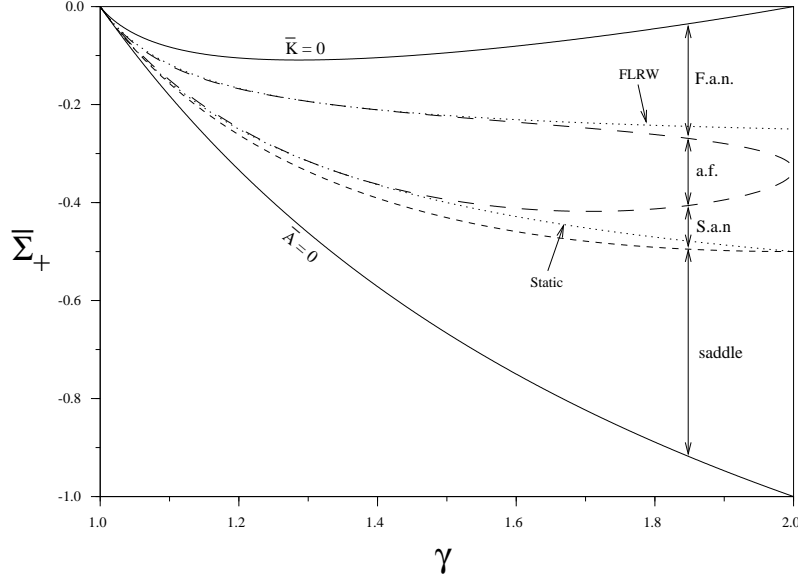


Figure 1. This figure shows the stability of the sonic line, parametrized by $\bar{\Sigma}_+$, for γ in the interval $1 < \gamma < 2$. The attractive nodal regions are denoted by F.a.n. and S.a.n., while the attractive focus is denoted by a.f. The full curves mark the boundaries of the physical interval for $\bar{\Sigma}_+$. The dotted curves are the values on the sonic line for the flat FLRW orbit and the static orbit, respectively. A similar figure was presented in [13].

Table 3. The various boundary submanifolds.

Boundary	Restriction
N^\pm	$u = \pm 1$
V	$\bar{\Sigma}_+ = 0, \Omega = 0$
${}_1\text{I}$	$\bar{K} = 0$
SV_\pm	$\bar{A} = 0, \Omega = 0, \text{sgn}(u) = \pm 1$
S	$\bar{A} = 0, u = 0$

3.2. Invariant submanifolds on the boundary of the TSS phase space

As stated previously, the boundary is described by a number of invariant subsets: $\Omega_t = 0, \bar{A} = 0, \bar{K} = 0, u = \pm 1$. The constraint (16) leads to $u\Omega_t = 0$ when $\bar{A} = 0$. For $u = 0$ one obtains the reduced equations for the static spherically symmetric perfect-fluid models. When $\Omega_t = 0, u \neq 0$ one obtains the static vacuum equations for a spherically symmetric space time with a test fluid. The submanifolds $u = \pm 1$ are described by the same equations as the TSS spherically symmetric model with a null (e.g. neutrino) fluid. The equations for the submanifold $\bar{K} = 0$ are the same as the reduced equations for the type ${}_1\text{I}$ models. The submanifolds are summarized in table 3 where we also introduce designations.

We will now describe the dynamical features of the individual boundary submanifolds.

The N^\pm submanifolds. These submanifolds correspond to Cauchy horizons that are black hole event horizons or, in a cosmological context, particle horizons [1].

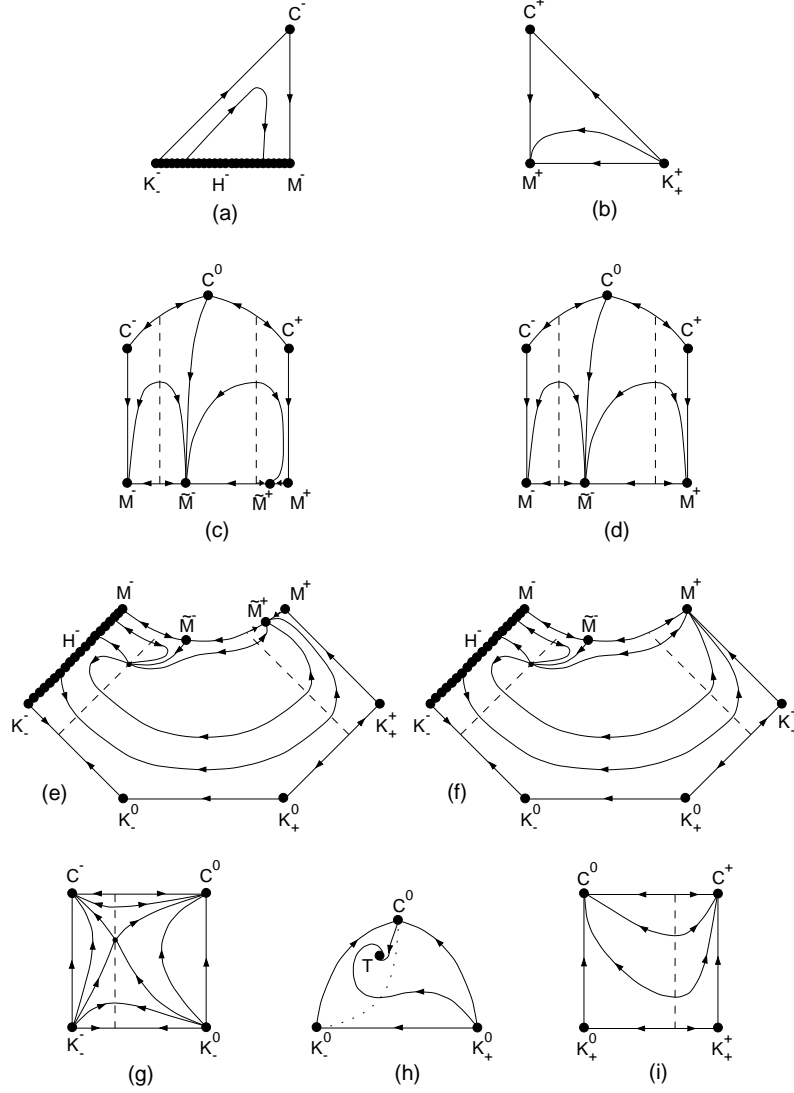


Figure 2. The phase portraits of the invariant submanifolds that constitute the boundary of the reduced phase space.

The dynamical structure of the N^- submanifold is given in figure 2(a) and the corresponding diagram for N^+ is given in figure 2(b). The N^\pm submanifolds are solvable. The integral describing the various orbits is given by

$$\frac{\bar{\Sigma}_+ \bar{A}}{[1 - \bar{\Sigma}_+ - \text{sgn}(u) \bar{A}]^2} = \text{constant}. \quad (27)$$

The vacuum V submanifold. The dynamical structure of the V submanifold is given in figure 2(c) ($\gamma < \frac{6}{5}$) and 2(d) ($\gamma \geq \frac{6}{5}$). Note that \bar{A} is an increasing monotonic function, which by the constraint implies that \bar{K} is a decreasing monotonic function.

The ${}_1\text{I}$ submanifold. The dynamical structure of the plane-symmetric type ${}_1\text{I}$ submanifold is given in figure 2(e) ($\gamma < \frac{6}{5}$) and 2(f) ($\gamma \geq \frac{6}{5}$).

The static vacuum SV_{\pm} submanifolds. The dynamical structure of the SV_- submanifold is given in figure 2(g) and the corresponding diagram for SV_+ is given in figure 2(i). The SV_{\pm} submanifolds are solvable. The integral describing the various orbits is given by

$$\frac{(1 - \bar{\Sigma}_+)^{3\gamma-2} u^{2(\gamma-1)} (1 - u^2)^{2-\gamma}}{(1 + \bar{\Sigma}_+)^{2-\gamma} \bar{\Sigma}_+^{4(\gamma-1)}} = \text{constant}. \quad (28)$$

The static S submanifold. The dynamical structure of the S submanifold is given in figure 2(h). There exists a monotonic function for this submanifold, excluding the point T . It can be found by using the Hamiltonian methods developed in ch 10 of [20]. It is given by

$$Z = \frac{(3\gamma - 2 + 2(\gamma - 1)\bar{\Sigma}_+)^2}{\Omega^p \bar{K}^q}, \quad p = \frac{4(\gamma - 1)^2}{(5\gamma - 4)\gamma}, \quad q = \frac{(\gamma^2 + 4(\gamma - 1))}{(5\gamma - 4)\gamma}, \quad (29)$$

with

$$\frac{Z'}{Z} = - \frac{2(3\gamma - 2) [2(\gamma - 1) + (3\gamma - 2)\bar{\Sigma}_+]^2}{[3\gamma - 2 + 2(\gamma - 1)\bar{\Sigma}_+] (5\gamma - 4)\gamma}. \quad (30)$$

This monotonic function prevents the existence of equilibrium points, periodic orbits, recurrent orbits and homoclinic orbits in this region, see e.g. [25]. The static spherically symmetric perfect-fluid models have been studied qualitatively by Collins using non-compact variables [26], but the above monotonic function is, to our knowledge, new. The compact formulation taken together with this monotonic function leads to a complete understanding of the dynamics of static spherically symmetric models. It is worth noting that the orbit from C^0 to T corresponds to the only regular solution which exists for these models (modulo a scale invariance parameter). As will be discussed in section 4.2, this orbit constitutes part of the boundary of a two-dimensional interior submanifold corresponding to regular self-similar solutions. The mass function (see Appendix A.2) for the S submanifold is

$$\frac{2m}{R} = 1 - \frac{(1 + \bar{\Sigma}_+)^2}{\bar{K}}. \quad (31)$$

The condition $m = 0$ defines a curve between K_-^0 and C^0 . This curve is indicated by the dotted curve in figure 2(h). Both the equilibrium point T and the regular solution C^0 - T are located in the $m \geq 0$ region. The corresponding solutions are the only static solutions which have a non-negative mass everywhere, since all other orbits come from K_+^0 , located in the $m < 0$ region.

4. Global behaviour

By appropriately ‘gluing together’ the boundary submanifolds of the previous section, we obtain the reduced phase space shown in figures 3 and 4. The TSS perfect-fluid models correspond to orbits in the interior reduced phase space. The ${}_1\text{I}$ submanifold makes up the bottom of a ‘tent’ with the other submanifolds as ‘walls’. The point C^0 is the top of the ‘tent’. Indicating the stability of the equilibrium points on the boundary,

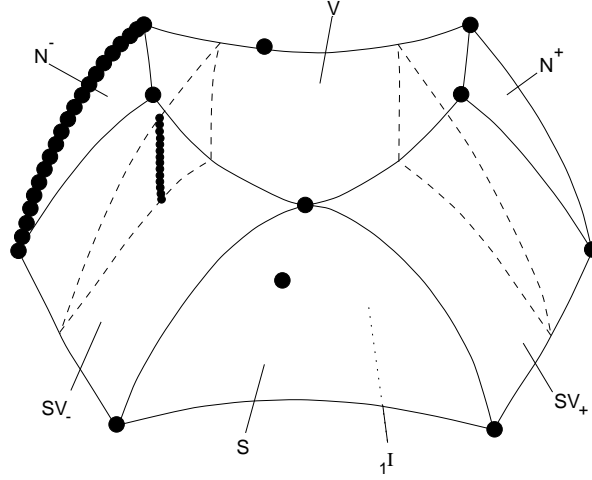


Figure 3. This picture shows how the boundary of the reduced phase space of the timelike self-similar spherically symmetric models is constructed out of the invariant submanifolds discussed in section 3.2. The broken curves describe the sonic surfaces.

we obtain figure 4 for $\gamma > \frac{6}{5}$. For $\gamma \leq \frac{6}{5}$, the point \tilde{M}^+ enters the physical phase space, but is always beyond the sonic surface located at $u = \sqrt{\gamma - 1}$. It is impossible to analytically continue solutions through the sonic surface there, in contrast to the one at $u = -\sqrt{\gamma - 1}$. Thus the bifurcation at $\gamma = \frac{6}{5}$ only affects the ‘physically uninteresting’ part of the phase space, $\sqrt{\gamma - 1} \leq u \leq 1$. The advantage of a compact and regular phase space is now apparent: no parts of the phase space are ‘crushed’. This is in contrast to, e.g., Bogoyavlensky [4], where parts of the phase space are cut off, while others are located at infinity.

The orbits on the boundary corresponding to the eigenvector directions of the points \tilde{M}^- and C^0 are shown in figure 4, as is the static orbit along the eigenvector direction of the point T pointing into the phase space. The two-dimensional separatrix surface entering the interior phase space from C^0 and bounded by these orbits will be discussed in section 4.2.

4.1. Monotonic functions

As indicated above, monotonic functions are important tools for understanding the global dynamics. The function [14]

$$F = \bar{K}^{2-\gamma} \bar{\Sigma}_+^{3\gamma-4} \bar{A}^{-\gamma} u^{-2(\gamma-1)} (1-u^2)^{-(2-\gamma)}, \quad (32)$$

whose derivative with respect to the independent variable η is

$$F' = \left[\frac{(2-\gamma)(3\gamma-2)(1-u^2)\bar{A}}{\gamma u} \right] F, \quad (33)$$

is easily seen to be monotonic in the regions $u < 0$ and $u > 0$. This monotonic function tells us that all orbits in the $u > 0$ part of the phase space come from the sonic surface at $u = \sqrt{\gamma - 1}$ [4]. Thus, all the ‘interesting’ dynamics takes place for $u < 0$.

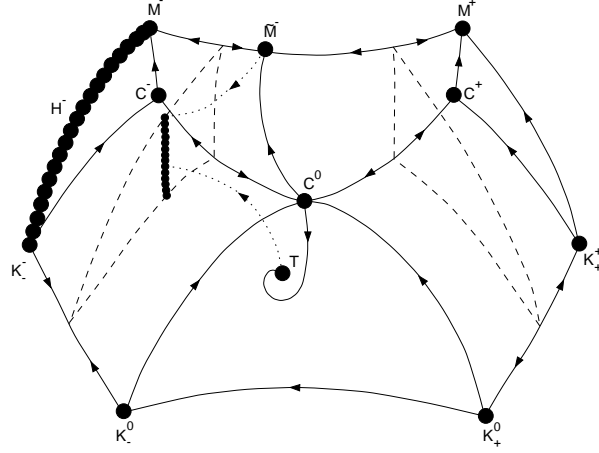


Figure 4. The global structure of the reduced phase space for $\gamma \geq \frac{6}{5}$. The orbits on the boundary corresponding to the eigenvector directions of the points \bar{M}^- and C^0 are shown, as is the static orbit along the eigenvector direction of the point T pointing into the phase space.

4.2. Invariant submanifolds in the interior of the TSS phase space

A number of trajectories, corresponding to exact solutions of the field equations, can be found.

The flat FLRW orbit. An orbit corresponding to the flat FLRW solution can be obtained by imposing the Petrov type 0 condition, $C = 0$ see equation (A.4), along with vanishing fluid shear. It is described by

$$\bar{\Sigma}_+ = -\frac{2u^2}{(3\gamma - 2) + 4u^2}, \quad \bar{A} = -\frac{3\gamma u}{(3\gamma - 2) + 4u^2}. \quad (34)$$

The flat FLRW orbit passes through the sonic line at an equilibrium point in the F.a.n. nodal region. The value of the variable $\bar{\Sigma}_+$ on the sonic line is given by the upper dotted curve in figure 1. The flat FLRW orbit approaches the sonic line along an eigendirection. Thus the flat FLRW solution is analytic across the sonic surface, as expected (for a discussion about differentiability, see the discussion about the ASL submanifold below). The corresponding eigendirection is primary for $\gamma < \frac{4}{3}$, and secondary for $\gamma > \frac{4}{3}$. This was pointed out in [3, 13].

The static orbit. The static orbit, discussed in a previous section, enters the physical phase space from the point T and can be found explicitly:

$$\bar{\Sigma}_+ = -\frac{2(\gamma - 1)}{3\gamma - 2}, \quad \bar{A} = -\frac{\gamma u}{3\gamma - 2}. \quad (35)$$

Note that the static solution is not the only solution that is represented both as an equilibrium point on the boundary and as a trajectory in the interior phase space. This is also the case with the flat FLRW solution in the SSS sector, see [15]. The static orbit passes through the sonic line at an equilibrium point in the S.a.n. nodal region. The value of the variable $\bar{\Sigma}_+$ on the sonic line is given by the lower dotted curve in figure 1. The static orbit approaches the sonic line along an eigendirection. Thus the

static solution is analytic across the sonic surface, as expected. The corresponding eigendirection is secondary for $\gamma < \frac{4}{3}$, and primary for $\gamma > \frac{4}{3}$.

The RC submanifold. A requirement on solutions describing collapse is that they should initially be regular at the origin. The point C^0 is associated with such a regular centre [3, 5, 13]. The outgoing eigendirections at this point span a surface which enters the reduced phase space. This one-parameter family of orbits will be denoted the *regular centre* or RC submanifold. Its boundary on the V submanifold is the orbit from C^0 , terminating at \tilde{M}^- (see figure 2(c) and (d)). The other boundary is the orbit from C^0 to T , continuing into the phase space along the static orbit. The orbits in the RC submanifold can be parametrized by the density at the centre. For example, Ori and Piran use a parameter D_0 (see Appendix B.3).

The closer an orbit starts to the $C^0 - T$ orbit the more it spirals around the static orbit. This is to be expected, since the T equilibrium point has a pair of complex eigenvalues. The circulation around the static orbit is associated with a sign change of the radial 3-velocity of matter v_R (see the expression in Appendix B.4). For orbits close to the static orbit, v_R changes sign several times. This corresponds to several collapsing and expanding spacetime regions enclosing each other. Thus solutions fall into different physical families depending on the number of zeroes n_v of v_R . This defines a band structure of the RC submanifold. Near the V submanifold we have ‘pure collapse’ solutions ($n_v = 0$). It is obvious that there is an infinite number of n_v -bands (since T has a pair of complex eigenvalues). The flat FLRW solution corresponds to an orbit within the RC submanifold, and belongs to the $n_v = 0$ n_v -band. The higher n_v -band structure corresponds to orbits close to the $C^0 - T$ orbit. These orbits and their continuation along the static orbit correspond to spacetimes that can be described in terms of self-similar coordinates as follows: the spacetime (the subsonic part) can be divided into two regions. In the first region the solution is approximated by the regular static solution multiplied by the homothetic factor. Thus the solution is approximately conformally static in this region. In the second region the solution is approximated by a perturbation of the static self-similar solution (written in conformally static form). This second regime thus corresponds to ‘quasi-static’ oscillations around the static solution. The static orbit itself is the only orbit starting at T , which implies that there are no asymptotically quasi-static solutions. However, there is a two-parameter set of solutions coming arbitrarily close to the static solution during a limited part of their evolution.

The intersection of the RC submanifold with the sonic surface exhibits another band structure in the following sense: when varying the density parameter D_0 it is found that there are continuous intervals of D_0 for which the orbits hit the sonic surface at the sonic line. The stability of the sonic line determines if an orbit correspond to a physically interesting solution. Consequently, ‘physical’ orbits must hit the sonic line in one of the nodal regions, or approach the sonic line along the attractive eigendirection of the saddle region. These bands were considered by Ori and Piran [3], and we will denote them OP-bands. One OP-band consists of orbits hitting the F.a.n. nodal region of the sonic line. This is the first band in Ori and Piran’s terminology. For $1 < \gamma \lesssim 1.04$, its upper boundary is an orbit approaching the sonic line along a secondary eigendirection of the F.a.n. nodal region. The corresponding solution is known as the general relativistic Penston-Larson (GRPL) solution [3]. For $1.04 \lesssim \gamma < \frac{4}{3}$, the boundary is the F.d.n. degenerate node. This is in accord with the proposition that orbits in the neighbourhood of the flat FLRW orbit meet the

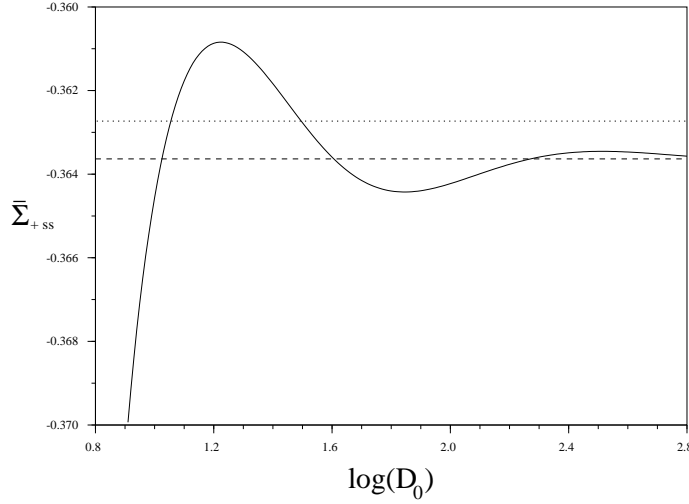


Figure 5. Values of $\bar{\Sigma}_+$ at the sonic surface for orbits with $\gamma = 1.4$. The broken line is the static value, and the dotted line is the S.d.n. degenerate node. One OP-band starts near the saddle region for $\log(D_0) \approx 0.81$ (not shown) and ends when the curve moves into the focal region at $\log(D_0) \approx 1.05$. This OP-band is the second band, using Ori and Piran's terminology. The third OP-band begins when the curve moves into the S.a.n. nodal region at $\log(D_0) \approx 1.5$. This OP-band is infinitely broad, as the curve never again moves into the focal region.

sonic surface along the sonic line for $\gamma < \frac{4}{3}$ [14]. For higher γ 's, the boundary is the flat FLRW orbit. The first OP-band is separated from higher OP-bands by a broad region where the orbits hit the sonic surface at other places than the sonic line. Orbits spiraling around the static orbit oscillate around the static value when they hit the sonic line. As discussed in connection with figure 1, the static orbit coincides with one of the degenerate nodes for $\gamma = \frac{4}{3}$. This implies that there will be a large number of OP-bands for equations of state with γ near $\frac{4}{3}$, because each time solutions move into the focal region on the sonic line, an OP-band ends with the S.d.n. degenerate node as boundary. When solutions move back into the S.a.n. nodal region, the next OP-band begins, again with the S.d.n. degenerate node as boundary, see figure 5. As D_0 increases, the amplitude of the oscillations decreases. Consequently, there is a value D_{0d} such that $D_0 > D_{0d}$ implies that orbits remain in the static nodal region. Thus, there is a finite number of OP-bands, except for $\gamma = \frac{4}{3}$ for which the static orbit coincides with the S.d.n. degenerate node. Note that the OP-band structure also is affected by whether the orbits hit the sonic surface on the sonic line or not. This is the dominant effect for creating OP-band structure for soft equations of state. For $1 < \gamma \lesssim 1.41$, the lower boundary of the second OP-band corresponds to an attractive eigendirection in the saddle region. For $1.41 \lesssim \gamma \lesssim 1.89$ the boundary is a secondary eigendirection in the S.a.n. nodal region, while for $\gamma \gtrsim 1.89$ it is the S.d.n. degenerate node (see also the discussion about critical behaviour below). The upper boundary changes character, depending on the value of γ . For $1 < \gamma \lesssim 1.11$, it is a secondary eigendirection in the S.a.n. nodal region. For $1.11 \lesssim \gamma \lesssim 1.45$, it is the S.d.n. degenerate node. The orbits in the second OP-band belong to n_v -band $n_v = 1$

or $n_v = 2$. For $\gamma \gtrsim 1.45$, the orbits never move into the focal region on the sonic line. The OP-band structure then degenerates to only two bands; the first OP-band, containing the flat FLRW solution, and a second band, infinitely broad in D_0 .

The ASL submanifold. In order for the solution to be analytic (or C^∞) at the sonic point, the corresponding orbit has to approach the sonic line along an eigendirection in one of the nodal regions [7, 12], or possibly along the attractive eigendirection in the saddle region. The corresponding orbits form a submanifold which we will call the ASL submanifold.

The RCASL submanifold. An analytic solution is regular at the centre and analytic at the sonic point. These solutions correspond to orbits that belong to the intersection of the RC and ASL submanifolds. This intersection forms a submanifold which we will denote as the RCASL submanifold. The RCASL submanifold turns out to be a discrete set of orbits. Typically, there is only one such solution for each n_v -band. A convenient numerical way to find orbits belonging to $RCASL = RC \cap ASL$ is to start along eigendirections at the sonic line. This gives a set of orbits in ASL. For an orbit belonging to RC, v_R should tend to zero, as $v_R = 0$ at C^0 . It is thus possible to ‘fork in’ the interesting solutions.

Foglizzo and Henriksen [13] use a set of variables particularly adapted to numerical studies of orbits between the sonic surface and the regular centre. However, we point out that their variables are non-compact and distort the global picture.

Criticality and self-similarity. Maison [9] and Hara *et al* [10, 27] consider the critical behaviour of spherically symmetric perfect-fluid collapse. A particular self-similar solution turns out to be of fundamental interest in these studies. This solution corresponds to an analytic orbit in the $n_v = 1$ n_v -band, and constitutes the lower boundary with respect to D_0 of the second OP-band for $1 \leq \gamma \lesssim 1.89$. For $\gamma \lesssim 1.41$ it approaches the sonic line in the saddle region along the attractive eigendirection. In the interval $1.41 \lesssim \gamma \lesssim 1.89$, it approaches the sonic line along a secondary eigendirection in the S.a.n. nodal region. For $\gamma \approx 1.61$, it passes through the point for which the static orbit reaches the sonic line. Above this value of γ , the zero in v_R occurs on the opposite side of the sonic point. For $\gamma \gtrsim 1.89$, the solution ends in the focal region, and thus becomes unphysical, see figure 6. The S.d.n. degenerate node is then the lower boundary of the second OP-band.

The F submanifold. For a global picture of self-similar spherically symmetric perfect fluid models, a careful study of the matching between the TSS and the SSS regions is necessary. In our previous work on the SSS region of the phase space [15], we studied a separatrix surface called the F submanifold. Orbits in this submanifold originate from an equilibrium point $+F$ in the SSS region of the phase space. This point corresponds to the flat FLRW solution and it gives the submanifold its name. However, the flat FLRW solution is not only represented as an equilibrium point on the boundary, but also as an orbit within the F submanifold (corresponding to a different foliation of the spacetime). The remaining orbits within the F submanifold correspond to models that are of considerable physical interest since they can be interpreted as density perturbations of the flat FLRW model. The F submanifold in the SSS region is divided into two parts; one corresponding to orbits lying entirely in

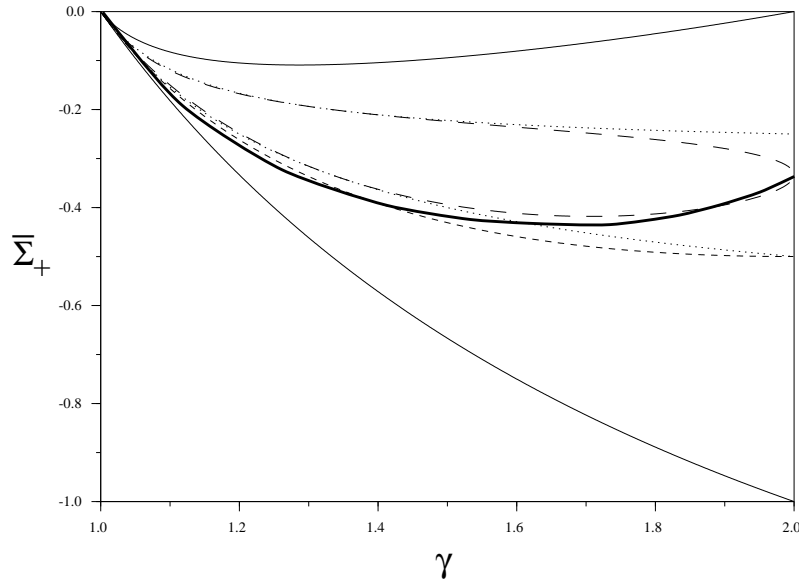


Figure 6. This figure shows the stability of the sonic line, parametrized by $\bar{\Sigma}_+$, for γ in the interval $1 < \gamma < 2$. The heavy full curve corresponds to the intersection of the critical solution with the sonic line. For other designations, see figure 1.

the SSS region and one corresponding to orbits reaching the \mathcal{H}^- line of equilibrium points (this equilibrium line is denoted ${}_{+}\mathcal{H}^-$ in the SSS region). This latter part of the F submanifold corresponds to solutions that can be analytically extended into the TSS region.

In order to connect the SSS and TSS phase spaces we use the variables of Foglizzo and Henriksen [13] (these variables arise in a comoving context and can therefore be used to deal with the situation where the self-similar symmetry surface becomes null, see Appendix B). Orbits corresponding to overdense solutions diverge from the flat FLRW orbit. Sufficiently overdense solutions re-enter the SSS region through \mathcal{H}^- and correspond to black hole solutions. However, there is a set of overdense orbits reaching the sonic surface.

Investigating the extendibility of orbits through the sonic surface, we find a band structure similar to the OP-band structure of the RC submanifold. We refer to these bands as *F-bands*. All underdense orbits, from the orbit in the ${}_1\text{I}$ submanifold to the orbit corresponding to the flat FLRW solution, pass the sonic surface through the sonic line. For $\gamma \geq \frac{4}{3}$ the limit of this band is the flat FLRW solution. For $\gamma < \frac{4}{3}$ there is a set of orbits corresponding to overdense solutions in this band. Between the first F-band and the next F-band there is a one-parameter subset of orbits that are inextendible and end at the sonic surface. This is similar to the region between the first and second OP-band of the RC submanifold. Between the subset of inextendible orbits and the orbits that return to the SSS region, there is a small band of orbits corresponding to overdense solutions that extend through the sonic surface via the sonic line. Our numerical investigation indicates that there is just one overdense F-band, rather than a hierarchy of several overdense bands (as was the case for the overdense OP-bands of RC for $\gamma \lesssim 1.45$). The interval of the sonic line corresponding

to the overdense F-band is wider than the corresponding interval covered by these OP-bands. Consequently, there are overdense subsonic ($u > -\sqrt{\gamma-1}$) solutions which are regular at the sonic surface, but cannot be connected with C^0 . Numerical analysis indicates that these orbits do not recollapse, but have a second irregular sonic point. Therefore, they are unphysical [13]. This is in accord with the conjecture of Carr and Coley [2] that asymptotically Friedmann solutions which contain black holes are supersonic everywhere.

Mass, energy and density fluctuations. The mass function $2m/R$ (see equation (A.5) in Appendix A.2) is a physically important quantity. By imposing the condition $m \geq 0$, only certain parts of the phase space are physical. In figure 2(h), the dotted line indicates the condition $m = 0$ in the static S submanifold (see the discussion of this submanifold in section 3.2).

Another interesting quantity is the asymptotic energy per unit mass E of a spherical shell (see equation (A.6) in Appendix A.2). Carr and Coley [1, 2] use this parameter in a general classification of self-similar spherically symmetric perfect fluids. We note that $E = 0$ for the flat FLRW solution, whereas the static solution has $E < 0$.

Self-similar density perturbations of the flat FLRW solution can be studied covariantly following Ellis and Bruni [28]. The fractional density gradient is characterized by a quantity L (see Appendix A.3). For the flat FLRW solution, L is zero, as expected. Orbits between the flat FLRW orbit and the V submanifold have $L > 0$ and correspond to under-dense solutions, while orbits on the other side of the flat FLRW orbit have $L < 0$, corresponding to overdense solutions.

5. Discussion

In this paper we have studied timelike self-similar spherically symmetric perfect-fluid models using a dynamical systems approach. It continues the work initiated in a previous paper, dealing with the spatially self-similar models. By suitably adapting the variables to the homothetic Killing vector, the reduced phase space for these models becomes compact and regular, a desirable property that has never been obtained before. An advantage of a compact and regular phase space is that it enables a more thorough global picture of the space of solutions. Also, the current local treatment of the constraint makes it possible to avoid ‘crushing’ parts of the phase space. The solution space of the TSS models has a much more complicated structure than in the SSS case. In particular, the existence of a sonic line in one of the sonic surfaces has profound implications for the global structure. The sonic surfaces and the sonic line act as ‘filters’ determining differentiability of various solutions.

To obtain a full global picture of self-similar spherically symmetric perfect-fluid models, it is necessary to match TSS and SSS regions. This has only been partially discussed here. A more complete discussion will be given in a subsequent paper. This will enable us to obtain a more detailed understanding of physical phenomena, such as formation of black holes and naked singularities.

By allowing an additional coordinate dependence in the metric coefficients, the approach of this paper can easily be generalized to non-self-similar spherically symmetric models. This is of interest when studying critical behaviour in spherically symmetric gravitational collapse. However, the field equations will now be partial differential equations, and the phase space will no longer be compact. Nevertheless, for small perturbations, this generalization of the present approach may be useful.

Acknowledgments

We wish to thank B J Carr and A A Coley for interesting discussions and for kindly providing us with access to unpublished manuscripts. CU was supported by the Swedish Natural Research Council.

Appendix A. Interesting physical quantities

Appendix A.1. Fluid properties and Petrov type conditions

The fluid expansion $\tilde{\theta}$, the fluid shear $\tilde{\sigma}$, the fluid acceleration scalar \tilde{a} and the Weyl scalar C are given by

$$\tilde{\theta} = \frac{e^{-t}}{\sqrt{3}(1-u^2)^{3/2}} \{u' + (1-u^2) [\bar{A} + (2 + \bar{\Sigma}_+)u]\} \bar{\theta}, \quad (\text{A.1})$$

$$\tilde{\sigma} = \frac{e^{-t}}{3(1-u^2)^{3/2}} |u' - (1-u^2)(1 + 2\bar{\Sigma}_+)u| \bar{\theta}, \quad (\text{A.2})$$

$$\tilde{a} = \frac{e^{-t}}{3\sqrt{3}(1-u^2)^{3/2}} |uu' + 3(1-u^2)(u\bar{A} - \bar{\Sigma}_+)| \bar{\theta}, \quad (\text{A.3})$$

$$C = \sqrt{C_{abcd}C^{abcd}} = \frac{2e^{-2t}}{3\sqrt{3}} |2\bar{\Sigma}'_+ - (1+q + \bar{\Sigma}_+)(1 + 2\bar{\Sigma}_+) + \bar{K}| (\bar{\mathcal{K}}, 4)$$

where q was defined in (14). Note that the magnetic part of the Weyl tensor is identically zero for all models. The spacetime is of Petrov type D if $C \neq 0$, and of type 0 if $C = 0$.

Appendix A.2. Mass and energy

For a general spherically symmetric spacetime the total mass-energy m between the centre distribution and some 2-space of symmetry is defined as (see, e.g., Misner and Sharp [29], Hernandez and Misner [30] and Cahill and McVittie [31])

$$\frac{2m}{R} = 1 - \tilde{g}^{ab} \frac{\partial R}{\partial x^a} \frac{\partial R}{\partial x^b} = \frac{\bar{K} - (1 + \bar{\Sigma}_+)^2 + \bar{A}^2}{\bar{K}}, \quad (\text{A.5})$$

where $R = e^t D_2(x)$ is the invariant radius of the symmetry surfaces. By definition, the matter is outside the gravitational radius $2m$ whenever $\frac{2m}{R} < 1$ and inside the gravitational radius when $\frac{2m}{R} > 1$. The latter case is associated with the existence of a black-hole apparent horizon or a cosmological apparent horizon at $R = 2m$.

It is possible to define the asymptotic energy per unit mass E of a spherical shell as [29]

$$E = \frac{1}{2} \left[U^2 - \frac{2m}{R} \right] = \frac{1}{2} \left[\frac{(1 + \bar{\Sigma}_+ + \bar{A}u)^2}{\bar{K}(1-u^2)} - 1 \right], \quad (\text{A.6})$$

where

$$U = \frac{1}{\sqrt{1-u^2}} \left(e^{-t} D_1^{-1} \frac{\partial}{\partial t} R + e^{-t} u \frac{\partial}{\partial x} R \right) = \frac{\bar{A} + u(1 + \bar{\Sigma}_+)}{\sqrt{\bar{K}}\sqrt{1-u^2}}. \quad (\text{A.7})$$

Appendix A.3. Density perturbations

A covariant approach to density perturbations has been given in [28]. The fractional density gradient is defined as

$$\Delta_a = \left(\frac{\Delta \tilde{\mu}}{\tilde{\mu}} \right)_a = \tilde{\mu}^{-1} \tilde{h}_a{}^b \tilde{\partial}_b \tilde{\mu}. \quad (\text{A.8})$$

In the reduced phase space variables, this leads to

$$\Delta_a = \bar{\theta} e^{-t} \frac{L}{1-u^2} (-u, 1, 0, 0), \quad (\text{A.9})$$

where

$$L = -\frac{2\bar{A}u[u^2 + (\gamma - 1)] + \gamma[2u^2 + (1 + u^2)\bar{\Sigma}_+]}{\sqrt{3}[u^2 - (\gamma - 1)]}. \quad (\text{A.10})$$

Appendix B. Coordinate and variable transformations

Here we will give transformations to other coordinates and variables which have been used in the literature to study self-similar spherically symmetric models. The present variables lead to a compact and regular description everywhere in the TSS sector. This is not the case with previously used variables, as is easily seen in the equations below. The simple algebraic relations make it easy to identify the points, or even manifolds, where breakdowns occur.

Appendix B.1. The variables used in the SSS region

In a previous paper [15], the form of the μ_n equation led us to compactify the variables with respect to $Y = \sqrt{\bar{\theta}^2 + 3\bar{B}_2^2}$ rather than $\bar{\theta}$. The resulting set of variables $(\bar{Q}_0, \bar{Q}_+, \bar{C}_1, v)$ are related to the variables used in this paper as follows:

$$\bar{Q}_0 = \frac{\text{sgn}(\bar{\theta})}{\sqrt{1+K}}, \quad \bar{Q}_+ = \frac{\bar{\Sigma}_+ \text{sgn}(\bar{\theta})}{\sqrt{1+K}}, \quad \bar{C}_1 = \frac{\bar{A} \text{sgn}(\bar{\theta})}{\sqrt{1+K}}, \quad v = u^{-1}. \quad (\text{B.1})$$

Note that since $\bar{\theta}$ is a dominant quantity in the TSS region, Y is even more dominant. Thus we could have compactified the variables in the TSS region in the same way as in the SSS region with the additional replacement $u = 1/v$. However, the present choice of compactification result in simpler equations. The TSS variables are of course not compact in the SSS region, as $\bar{\theta}$ is not a dominant quantity there. This is easily seen in the above relations.

Appendix B.2. Bogoyavlensky's variables

Bogoyavlensky uses the homothetic approach, solves the constraint globally, and introduces the variables Q, w and u (as a starting point) [4]. This results in an undesirable ‘crushing’ of the phase space. Bogoyavlensky’s variables are related to the present ones by

$$Q = \frac{\bar{A}}{1 + \bar{\Sigma}_+}, \quad w = -\frac{2\bar{\Sigma}_+}{1 + \bar{\Sigma}_+}. \quad (\text{B.2})$$

Appendix B.3. The comoving (fluid) approach

As the fluid 4-velocity singles out a preferred timelike direction in the spacetime, it should be beneficial to adapt the coordinates to this direction. The line element can be written as

$$ds^2 = -e^{\Psi(\lambda)} dT^2 + e^{\Lambda(\lambda)} dX^2 + Y(\lambda)^2 T^2 d\Omega^2, \quad (\text{B.3})$$

where $\lambda = T/X$ and $d\Omega^2 = d\theta^2 + \sin^2 \theta d\varphi^2$. By defining $T = \exp[t - F(\bar{x})]$, $X = \exp[t - F(\bar{x}) + \bar{x}]$, where the function $F(\bar{x})$ satisfies

$$\frac{dF}{d\bar{x}} = -\frac{e^{\Lambda+2\bar{x}}}{e^{\Psi} - e^{\Lambda+2\bar{x}}}, \quad (\text{B.4})$$

the line element equation (B.3) can be written as

$$ds^2 = e^{2t} (-D_1^2 dt^2 + N^2 d\bar{x}^2 + D_2^2 d\Omega^2) \quad (\text{B.5})$$

with

$$D_1^2 = e^{-2F} (e^{\Psi} - e^{\Lambda+2\bar{x}}), \quad N^2 = \frac{e^{\Lambda+2\bar{x}+\Psi-2F}}{e^{\Psi} - e^{\Lambda+2\bar{x}}}, \quad D_2^2 = e^{-2F} Y^2. \quad (\text{B.6})$$

Using that the fluid velocity is given by $u^2 = e^{\Lambda-\Psi+2\bar{x}}$, the above formulas can be written as

$$\frac{dF}{d\bar{x}} = -\frac{u^2}{1-u^2}, \quad D_1^2 = e^{\Psi-2F} (1-u^2), \quad N^2 = \frac{u^2 e^{\Psi-2F}}{1-u^2}, \quad (\text{B.7})$$

with D_2 the same as previously. The comoving approach has been used by many authors. The most useful variables produced so far to study self-similar spherically symmetric collapse of a perfect fluid in this approach are probably the ones obtained by Foglizzo and Henriksen [13] (see also Bicknell and Henriksen [7, 12]). Their variables $\{N_{F-H}, \mu_{F-H}, v_{F-H}\}$ are related to the present ones by

$$N_{F-H} = \frac{3\gamma\bar{\Sigma}_+}{2u\bar{A}}, \quad \mu_{F-H} = \frac{3\gamma u (\bar{K} - (1 + \bar{\Sigma}_+)^2 + \bar{A}^2)}{2(1-u^2)\bar{\Sigma}_+\bar{A}}, \quad (\text{B.8})$$

and $v_{F-H} = u$. Here, we eliminated μ_t using the constraint equation (8). Note the close connection between μ_{F-H} and the mass function (A.5). Again it is obvious that these variables are not compact. However, they are useful for connecting the SSS and TSS regions and they are also very well suited for studying the phase space in the vicinity of the sonic line.

Appendix B.4. The Schwarzschild approach

One often represents a spherically symmetric line-element with its ‘Schwarzschild’ form:

$$ds^2 = -FdT^2 + GdR^2 + R^2 d\Omega^2, \quad (\text{B.9})$$

where, in the self-similar case, F and G are functions of R/T only. By introducing $R = e^t B_2^{-1}$, $T = e^t e^\phi$, where the function ϕ satisfies the differential equation

$$\frac{d\phi}{dx} = \frac{\bar{A}^2 \bar{\theta}}{\sqrt{3} (1 + \bar{\Sigma}_+)}, \quad (\text{B.10})$$

the line element (B.9) transforms into the diagonal homothetic form. The metric functions F and G become

$$F = \frac{3(1 + \bar{\Sigma}_+)^2 e^{-2\phi} \bar{\theta}^{-2}}{\bar{A}^2 \left[(1 + \bar{\Sigma}_+)^2 - \bar{A}^2 \right]}, \quad G = \frac{\bar{K}}{(1 + \bar{\Sigma}_+)^2 - \bar{A}^2}. \quad (\text{B.11})$$

Defining $G^{-1} = 1 - 2m/R$ recovers the definition of the mass function (A.5). The radial 3-velocity of matter v_R , i.e. the speed of the fluid with respect to the surfaces $R = \text{constant}$, is given by

$$v_R = \frac{\bar{A} + u(1 + \bar{\Sigma}_+)}{1 + \bar{\Sigma}_+ + u\bar{A}}. \quad (\text{B.12})$$

The Schwarzschild approach has been used by several authors. The variables of Ori and Piran [3] are given by

$$\mathcal{M} = \frac{\bar{K} - (1 + \bar{\Sigma}_+)^2 + \bar{A}^2}{2\bar{K}}, \quad D = \frac{(1 - u^2) \bar{\Sigma}_+ \bar{A}}{\gamma \bar{K} u}, \quad (\text{B.13})$$

$$u^r = \frac{\bar{A} + u(1 + \bar{\Sigma}_+)}{\sqrt{(1 - u^2) \bar{K}}}.$$

The orbits in the RC submanifold are parametrized by

$$D_0 \equiv \lim_{R/T \rightarrow 0} \frac{D}{(R/T)^2}. \quad (\text{B.14})$$

The sonic line is subsequently parametrized by the variable $Y = \mathcal{M}/RD$ which on the sonic line is just

$$Y = \frac{-2(\gamma - 1)\bar{\Sigma}_+}{2(\gamma - 1) + \gamma\bar{\Sigma}_+}. \quad (\text{B.15})$$

This approach was also used by Maison [9] for studying the more general problem of non-universality in non-self-similar gravitational collapse. He used a set of variables $(A_M, B_M, \bar{\rho}_M, v_M)$. In their renormalization group approach to the critical behaviour of spherically symmetric collapse, Hara *et al* [10] used a set of variables (N_H, A_H, ω_H) very similar to the variables of Maison (however, they solve the constraint globally). In the self-similar case, these sets of variables are given by

$$A_M^2 = A_H^{-1} = \frac{(1 + \bar{\Sigma}_+)^2 - \bar{A}^2}{\bar{K}}, \quad B_M^2 = N_H^{-2} = \frac{\bar{A}^2}{(1 + \bar{\Sigma}_+)^2}, \quad (\text{B.16})$$

$$\bar{\rho}_M = \frac{\omega_H}{A_H} = \frac{(1 - u^2) \bar{\Sigma}_+ \bar{A}}{\gamma \bar{K} u}, \quad v_M = V_H = v_R.$$

References

- [1] Carr B J and Coley A A 1997 A complete classification of spherically symmetric perfect-fluid similarity solutions *Preprint*
- [2] Carr B J and Coley A A 1997 Self-similarity in general relativity *Preprint*
- [3] Ori A and Piran T 1990 *Phys. Rev. D* **42** 1068
- [4] Bogoyavlensky O I 1985 *Methods in the Qualitative Theory of Dynamical Systems in Astrophysics and Gas Dynamics* (Berlin: Springer)
- [5] Carr B J and Yahil A 1990 *Astrophys. J.* **360** 330
- [6] Carr B J and Hawking S W 1974 *Mon. Not. R. Astron. Soc.* **168** 399
- [7] Bicknell G V and Henriksen R N 1978 *Astrophys. J.* **219** 1043

- [8] Evans C R and Coleman J S *Phys. Rev. Lett.* **72** 1782
- [9] Maison D 1996 *Phys. Lett.* **366B** 82
- [10] Koike T, Hara T and Adachi S 1995 *Phys. Rev. Lett.* **74** 5170
- [11] Cahill M E and Taub A H 1971 *Commun. Math. Phys.* **21** 1
- [12] Bicknell G V and Henriksen R N 1978 *Astrophys. J.* **225** 237
- [13] Foglizzo T and Henriksen R N 1993 *Phys. Rev. D* **48** 4645
- [14] Anile A M, Moschetti G and Bogoyavlenski O I 1987 *J. Math. Phys.* **28** 2942
- [15] Goliath M, Nilsson U S and Uggla C 1998 *Class. Quantum Grav.* **15** 167
- [16] Kramer D, Stephani H, MacCallum M and Herlt E 1980 *Exact Solutions of Einstein's Field Equations* (Cambridge: Cambridge University Press)
- [17] Nilsson U and Uggla C 1996 *Class. Quantum Grav.* **13** 1601
- [18] Nilsson U S and Uggla C 1997 *Class. Quantum Grav.* **14** 1965
- [19] Hewitt C G and Wainwright J 1992 *Phys. Rev. D* **46** 4242
- [20] J Wainwright and G F R Ellis (eds.) 1997 *Dynamical systems in cosmology* (Cambridge: Cambridge University Press)
- [21] Tolman R C 1939 *Phys. Rev.* **55** 364
- [22] Oppenheimer J R and Volkoff G M 1939 *Phys. Rev.* **55** 374
- [23] Klein O 1947 *Ark. Mat. Astr. Fys. A* **34** (19) 1
- [24] Misner C W and Zapsky H S 1964 *Phys. Rev. Lett.* **12** 635
- [25] Wainwright J and L Hsu 1989 *Class. Quantum Grav.* **6** 1409
- [26] Collins C B 1985 *J. Math. Phys.* **26** 2268
- [27] Hara T, Koike T and Adachi S *Preprint* gr-qc/9607010
- [28] Ellis G F R and Bruni M 1989 *Phys. Rev. D* **40** 1804
- [29] Misner C W and Sharp D H 1964 *Phys. Rev. B* **136** 571
- [30] Hernandez W C and C W Misner 1966 *Astrophys. J.* **143** 452
- [31] Cahill M E and G C McVittie 1970 *J. Math. Phys.* **11** 1382